**Supporting Information**

# Thermally Stable Perovskite Solar Cells with Efficiency over 21% via Bifunctional Additive

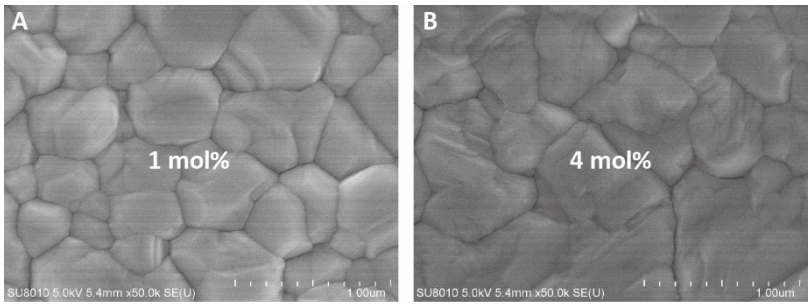


**Figure S1.** Top-view SEM images of perovskite films with biuret additive.

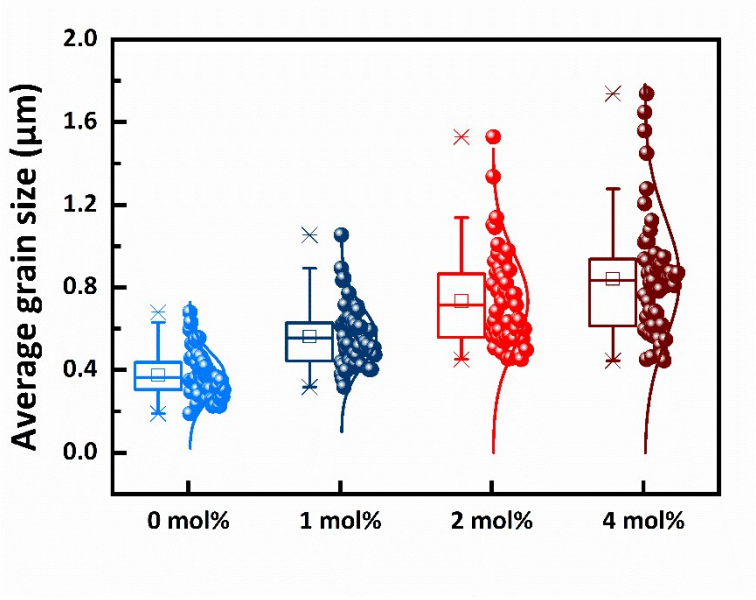


**Figure S2.** Average grain size obtained from corresponding SEM images in Figure S1 using *Nano Measurer* (version 1.2) software.

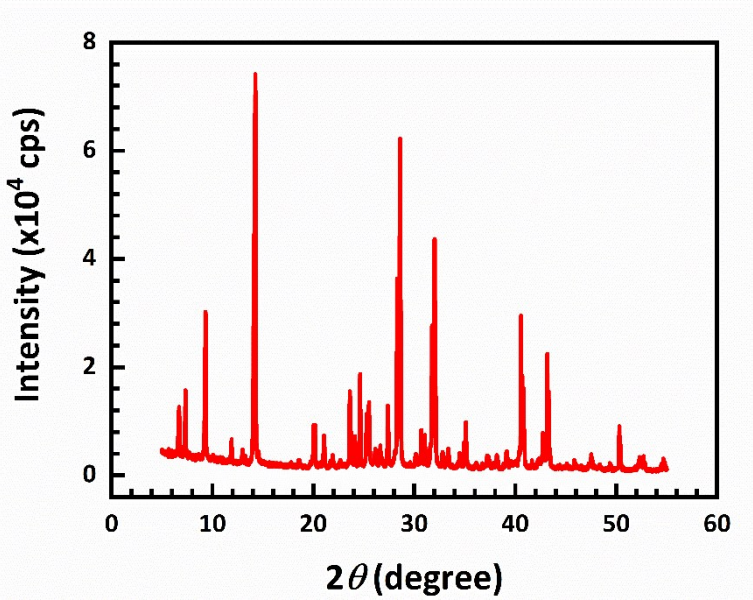


**Figure S3.** XRD pattern of (MAI)·$PbI_2$·DMSO·biuret adduct.

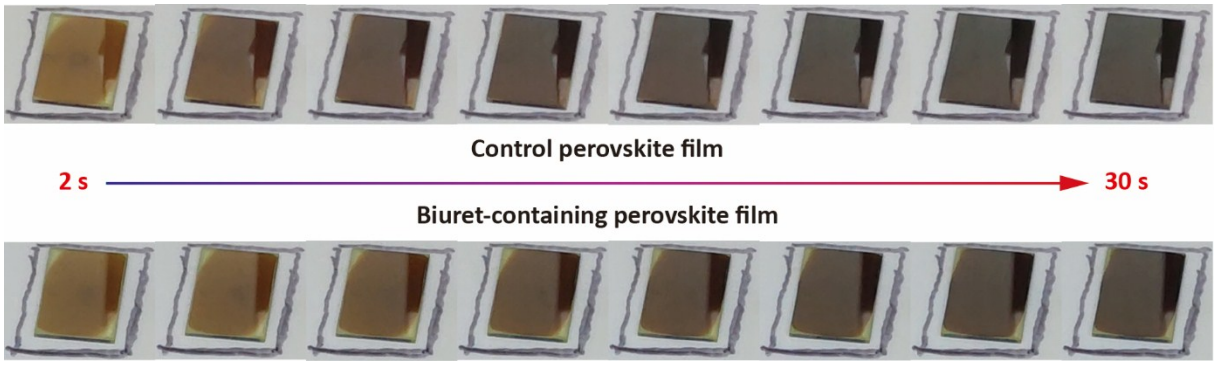


**Figure S4.** Photographs of perovskite films during crystallization at 100 °C.

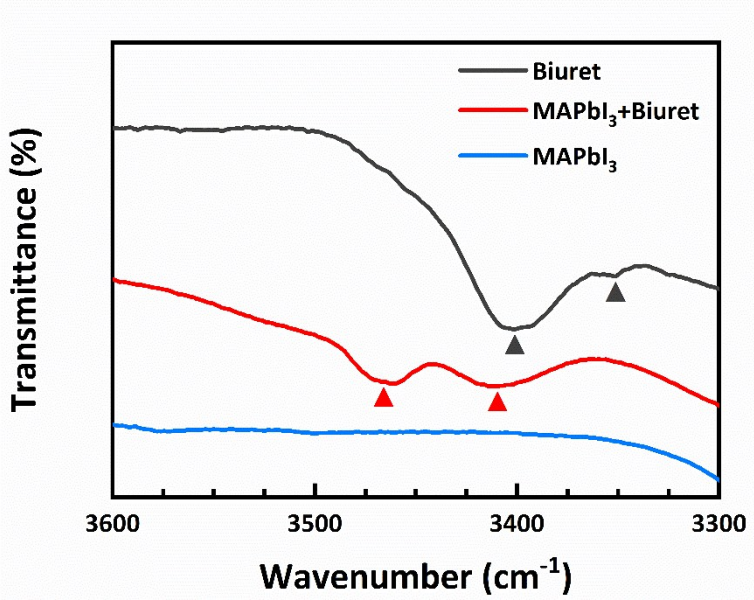


**Figure S5.** Enlarged fingerprint region in the ATR-FTIR spectra for the N-H stretch.

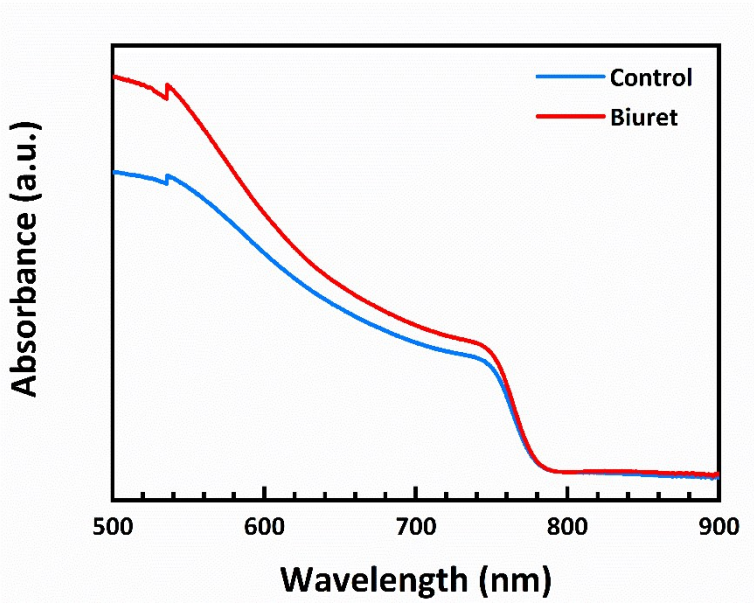


**Figure S6.** UV-vis absorption spectra of perovskite films with and without biuret additive.

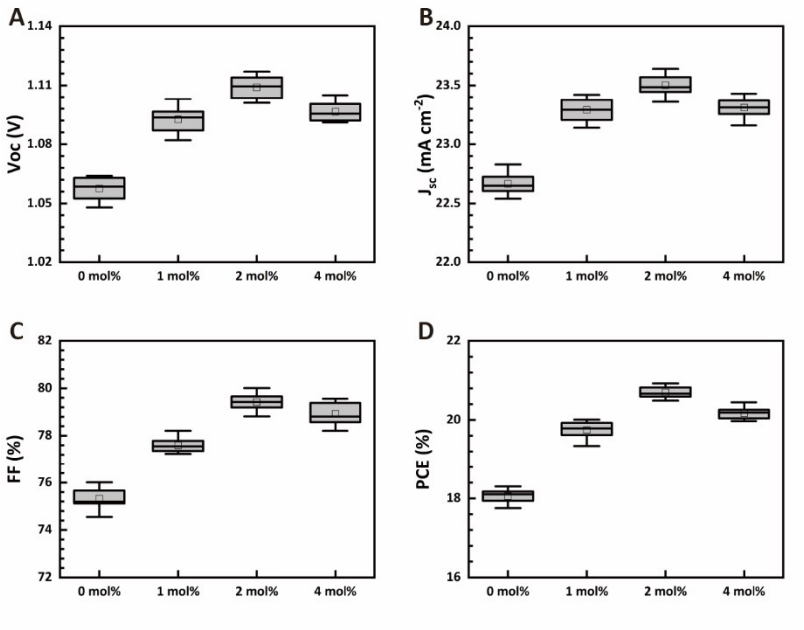


**Figure S7.** Photovoltaic parameters of $MAPbI_3$ solar cells (12 devices for each case) as a function of the amount of biuret additive.

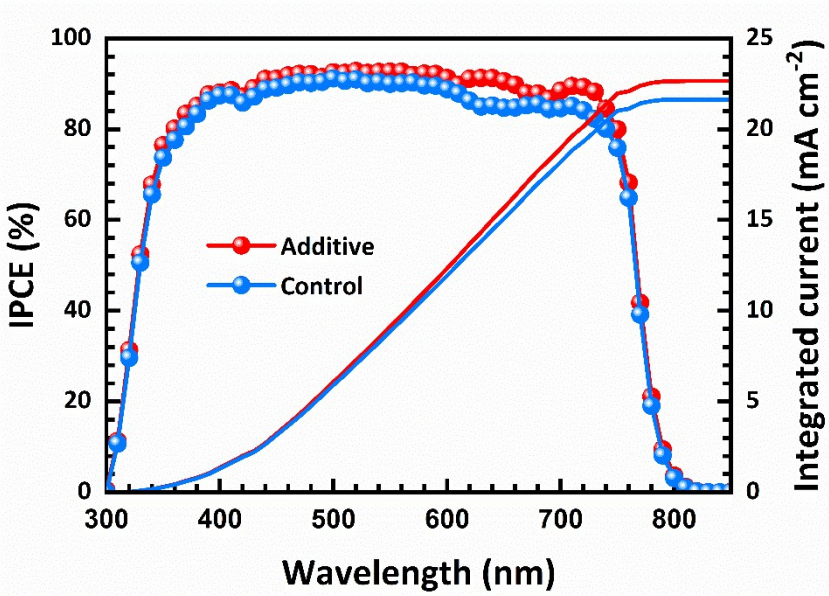


**Figure S8.** IPCE curves and integrated $J_{sc}$ of the champion devices.

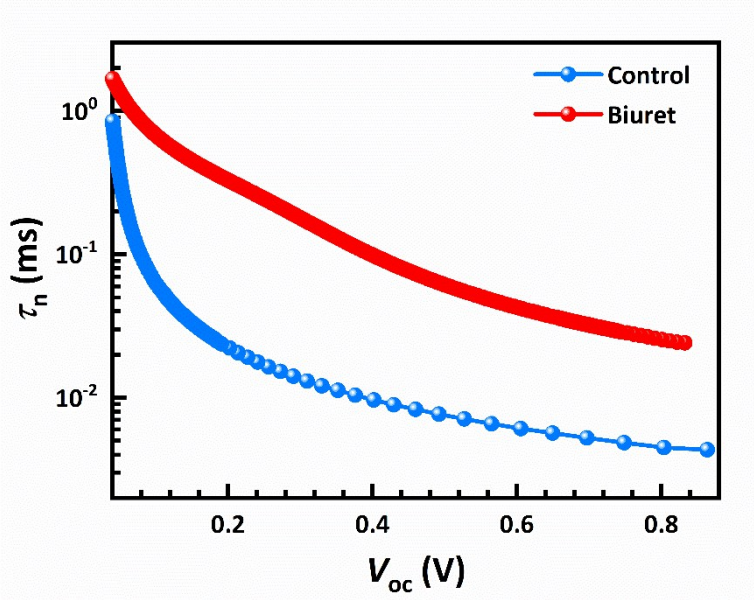


**Figure S9.** The calculated electron lifetime of control and biuret-modified devices.

**Table S1.** Photovoltaic parameters of $MAPbI_3$ solar cells with different amounts of biuret additive. Parameters were averaged over 12 individual devices.

| Devices | $J_{sc}$ (mA cm$^{-2}$) | $V_{oc}$ (V) | FF (%) | PCE (%) |
|---|---|---|---|---|
| 0 mol% | 22.67 ± 0.09 | 1.06 ± 0.01 | 75.33 ± 0.42 | 18.06 ± 0.17 |
| 1 mol% | 23.29 ± 0.10 | 1.09 ± 0.01 | 77.59 ± 0.29 | 19.74 ± 0.22 |
| 2 mol% | 23.50 ± 0.08 | 1.11 ± 0.01 | 79.42 ± 0.37 | 20.70 ± 0.75 |
| 4 mol% | 23.31 ± 0.08 | 1.10 ± 0.01 | 78.92 ± 0.47 | 20.17 ± 0.14 |

**Table S2.** Photovoltaic parameters of $MAPbI_3$ solar cells with and without biuret additive measured under different scan directions.

| Devices | Scan direction | $J_{sc}$ (mA cm$^{-2}$) | $V_{oc}$ (V) | FF (%) | PCE (%) | HI |
|---|---|---|---|---|---|---|
| Control | Reverse | 22.38 | 1.06 | 76.32 | 18.15 | 0.086 |
| | Forward | 22.41 | 1.03 | 71.94 | 16.59 | |
| Biuret | Reverse | 23.47 | 1.11 | 79.65 | 20.84 | 0.004 |
| | Forward | 23.64 | 1.11 | 79.17 | 20.76 | |

**Table S3.** Summary of the reported device performance of $MAPbI_3$ solar cells.

| Device structure | Advanced strategies | PCE | Year | Ref. |
|---|---|---|---|---|
| ITO/**PEDOT:PSS/$MAPbI_3$**/$C_{60}$/BCP/Ag | Post treatment | 21.06% | *ACS Nano* 2018 | Chiang et al[1] |
| ITO/**PTAA/$MAPbI_3$**/$C_{60}$/BCP/Cu | Additive engineering | 21.5% | *Joule* 2019 | Zheng et al[2] |
| ITO/**PTAA/Single-Crystal $MAPbI_3$**/$C_{60}$/BCP/Cu | | 21.09% | *ACS Energy Lett.* 2019 | Chen et al[3] |
| FTO/**cp-$TiO_2$/$MAPbI_3$**/Spiro-OMeTAD/$MoO_3$/Ag | Additive engineering | 20.4% | *Adv. Mater.* 2019 | Li et al[4] |
| FTO/**$TiO_2$ nanowire/$MAPbI_3$**/Spiro-OMeTAD/Au | Contact engineering | 21.10% | *Small* 2019 | Wu et al[5] |
| FTO/**cp-$TiO_2$/mp-$TiO_2$/$MAPbI_3$**/Spiro-OMeTAD/Au | Interface engineering | 20.4% | *Adv. Mater.* 2019 | Chen et al[6] |
| FTO/**cp-$SnO_2$/$MAPbI_3$**/Spiro-OMeTAD/Ag | Contact engineering | 20.52% | *Adv. Funct. Mater. 2019* | Chen et al[7] |
| FTO/**cp-$SnO_2$/mp-$SnO_2$/$MAPbI_3$**/spiro/Au | Contact engineering | 19.12% | *Adv. Funct. Mater. 2018* | Xiong et al[8] |
| FTO/**cp-$TiO_2$/mp-$TiO_2$/$MAPbI_3$**/Spiro-OMeTAD/Au | Additive engineering | 21.16% | **This work** | |

Table S3 summarizes the photovoltaic efficiency of the reported high-performance $MAPbI_3$ solar cells. The reported champion PCE of $MAPbI_3$ solar cells with different structures were displayed. A promissing PCE of 21.16% is reported in this work which to our knowledge is the highest efficiency for $MAPbI_3$ solar cells with a mesoporous electron transport layer. Moreover, the obtained PCE here is even comparable with the PCE of the single-crystal $MAPbI_3$ solar cells. (note that cp means compact, mp means mesoporous)

**Note 1: Crystallite Size Caculation Based on Scherrer Equation**

$$D = \frac{K\lambda}{B\cos\theta}$$

Here $D$ represents the average crystallite grain diameter (nm), $K$ is the proportionality constant, $\lambda$ is the wavelength of the X-ray irradiation (0.154 nm), and $B$ is the full width at half maximum (FWHM) (in radians). We calculated the crystallite size using the FWHM of the (110) peak. We assume a proportionality constant of $K$ = 0.94, which is appropriate if the crystallites are roughly spherical in shape.

$$D = \frac{K\lambda}{B\cos\theta} = \frac{0.94 \times 0.154}{B \times \frac{\pi}{180} \times \cos\left(14.1^{\circ}\right)} = \frac{8.555}{B}$$

From an analysis using the Scherrer equation, the crystal sizes of control and biuret-modified perovkites are estimated to be 51.8 nm and 66.3 nm, respectively. It is important to note that these values are based on the assumption of spherical perovskite crystals. In contrast, for our samples, because of the film thickness limitation, crystals are much more parallel than perpendicular to the substrate, meaning that the crystal size is underestimated by the Scherrer equation analysis. Considering that all samples have similar film thickness, it is safe to assume that the observed size trend is still valid.

**Experimental Section**

**Materials**

FTO glass (15 Ω/sq) was purchaesd from South China Science & Technology Company Limited. Titanium diisopropoxide bis(acetylacetonate) was obtained from Sigma-Aldrich. Methylammonium iodide (MAI, >98.0%(N)), lead (II) iodide ($PbI_2$, 99.99%), and biuret (>99.0%(N)) were purchased from TCI Chemicals. 2,2′,7,7′-Tetrakis-(*N,N*-di-*p*methoxyphenylamine)9,9′-spirobifluorene (Spiro-OMeTAD), 4-tert-butylpyridine (tBP), lithium bis(trifluoromethanesulfonyl)imide (Li-TFSI), and tris(2-(1H-pyrazol-1-yl)-4-tert-butylpyridine)-cobalt(III) tris(bis(trifluoromethylsulfonyl)imide) (FK209) were purchased from Xi'an Polymer Light Technology Corp. [6,6]-Phenyl-C61-butyric acid methyl ester (PCBM, >99.5%) was purchased from Lumtec. Anhydrous solvents, such as

dimethylformamide (DMF), dimethyl sulfoxide (DMSO), chlorobenzene (CB), isopropanol (IPA), and acetonitrile (ACN), were obtained from Alfa Aesar. All the chemicals were used as received without further purification.

**Device fabrication**

The $TiO_2$ compact layer was prepared by spraying a solution containing 1 mL of titanium diisopropoxide bis(acetylacetonate) and 7 mL of isopropanol on cleaned and patterned FTO substrates at 460°C using dry air as the carrier gas. Subsequently, the mesoporous $TiO_2$ layer was spin-coated onto the $TiO_2$ compact layer using diluted pastes and calcined at 510°C for 30 min in air to remove organic components. $TiO_2$ paste was prepared according to previously reported procedures.[9] The $MAPbI_3$ precursor solution was prepared by dissolving 461 mg of $PbI_2$ and 159 mg of MAI in 700 μL of DMF and 70 μL of DMSO, which was then spin-coated on the $TiO_2$ mesoporous layer at 4000 rpm (acceleration of 2000 rpm/s) for 30 s, to which 150 μL of CB was poured onto the spinning substrate 20 s prior the end of the program. For the device with biuret, different amount of biuret was added to the precursor solution. The perovskite films were then annealed on a hotplate at 100°C for 15 min. Once cooled down to room temperature, the hole transport layer was deposited on top of the perovskite layer by spin coating the Spiro-OMeTAD solution at 4000 rpm for 30 s. The Spiro-OMeTAD solution was prepared by dissolving 73.53 mg (60 mM) of Spiro-OMeTAD in 1 mL chlorobenzene, with the addition of 29.30 μL (200 mM) of tBP and 17.23 μL (30 mM) of Li-TFSI solution (500 mg Li-TFSI in 1 mL acetonitrile). Then, 6.78 μL (1.8 mM) of FK209 solution (400 mg FK209 in 1 mL acetonitrile) was added to the Spiro-OMeTAD solution; the molar ratio for FK209 and Spiro-OMeTAD was 0.03. Finally, a 100 nm gold layer was thermally evaporated on top of the device.

**Characterization**

The morphology and crystal structure of the perovskite films were characterized by SEM (SU8010, Hitachi) and XRD (Smartlab SE, Rigaku), respectively. ATR-FTIR measurements were conducted with the FTIR spectroscope (IRTracer-100, Shimadzu). XPS were carried out on the multifunctional photoelectron spectrometer (ESCALAB 250Xi, Thermo Scientific). The

absorption spectra of the perovskite films were measured on a UV-Vis spectrometer (UV-3600Plus, Shimadzu). Steady-state PL and PL mapping was performed on a home-built system as described elsewhere.[10] The *J-V* curves were recorded using a Keithley 2400 source meter under simulated sunlight from Newport AAA solar simulator (AM 1.5, 100 mW $cm^{-2}$). The active area of the device was defined as 0.1225 $cm^2$ with a nonreflective metal mask. IPCE spectra was measured as a function of wavelength from 300 to 900 nm (Enli Technology) with dual Xenon/quartz halogen light source.

**Reference**


1. C.-H. Chiang and C.-G. Wu, *ACS Nano*, 2018, **12**, 10355-10364.
2. X. Zheng, J. Troughton, N. Gasparini, Y. Lin, M. Wei, Y. Hou, J. Liu, K. Song, Z. Chen, C. Yang, B. Turedi, A. Y. Alsalloum, J. Pan, J. Chen, A. A. Zhumekenov, T. D. Anthopoulos, Y. Han, D. Baran, O. F. Mohammed, E. H. Sargent and O. M. Bakr, *Joule*, 2019, **3**, 1963-1976.
3. Z. Chen, B. Turedi, A. Y. Alsalloum, C. Yang, X. Zheng, I. Gereige, A. AlSaggaf, O. F. Mohammed and O. M. Bakr, *ACS Energy Lett.*, 2019, **4**, 1258-1259.
4. M. Li, Y.-G. Yang, Z.-K. Wang, T. Kang, Q. Wang, S.-H. Turren-Cruz, X.-Y. Gao, C.-S. Hsu, L.-S. Liao and A. Abate, *Adv. Mater*, 2019, **31**, 1901519.
5. W.-Q. Wu, J.-F. Liao, Y. Jiang, L. Wang and D.-B. Kuang, *Small*, 2019, **15**, 1900606.
6. H. Chen, T. Liu, P. Zhou, S. Li, J. Ren, H. He, J. Wang, N. Wang and S. Guo, *Adv. Mater*, 1905661.
7. C. Chen, Y. Jiang, J. Guo, X. Wu, W. Zhang, S. Wu, X. Gao, X. Hu, Q. Wang, G. Zhou, Y. Chen, J.-M. Liu, K. Kempa and J. Gao, *Adv. Funct. Mater.*, 2019, **29**, 1900557.
8. L. Xiong, M. Qin, C. Chen, J. Wen, G. Yang, Y. Guo, J. Ma, Q. Zhang, P. Qin, S. Li and G. Fang, *Adv. Funct. Mater.*, 2018, **28**, 1706276.
9. X. Shi, Y. Ding, S. Zhou, B. Zhang, M. Cai, J. Yao, L. Hu, J. Wu, S. Dai and M. K. Nazeeruddin, *Adv. Sci.*, 2019, **6**, 1901213.
10. X. Shi, R. Chen, T. Jiang, S. Ma, X. Liu, Y. Ding, M. Cai, J. Wu and S. Dai, *Sol. RRL*, 2020, **4**, 1900198.